

# Effects of a large mesospheric temperature enhancement on the hydroxyl rotational temperature as observed from the ground

Stella M. L. Melo<sup>1</sup> and R. P. Lowe

University of Western Ontario, London, Ontario, Canada

W. R. Pendleton Jr. and M. J. Taylor

Space Dynamics Laboratory and Physics Department, Utah State University, Logan, Utah, USA

B. Williams and C. Y. She

Colorado State University, Fort Collins, Colorado, USA

**Abstract.** The rotational temperature obtained from the rotational population distribution in the bands of the hydroxyl airglow has been shown to be a suitable proxy for the temperature at a height of 87 km [*She and Lowe, 1998*]. In this paper we examine in detail simultaneous observations on November 2–3, 1997, at Fort Collins, Colorado (41°N, 105°W), with both a sodium temperature lidar and the Coupling, Energetics, and Dynamics of Atmospheric Regions (CEDAR) OH mesospheric temperature mapper during which significant differences between the hydroxyl and lidar temperatures occur. The large differences are associated with a major temperature enhancement in the region of the peak of the hydroxyl emission. We model the effect on the shape of the emission rate profile of the hydroxyl airglow caused by the large temperature enhancement observed on this night by the lidar. As a result of the temperature sensitivity of the processes that give rise to the airglow, the profile shows major distortions from its normal shape. These distortions in turn lead to hydroxyl rotational temperatures that differ significantly from the 87-km lidar observations. The mean rotational temperature deduced in this way agrees well with the observed values. Such deviations in the temperature are expected to be rare, occurring only when a large temperature enhancement occurs near the peak of the airglow emission profile.

## 1. Introduction

Measurements of the relative intensities of rotational lines in the spectrum of molecular airglow emissions constitute one of the earliest techniques for remotely sensing the atmospheric temperature in the upper mesosphere region [*Meinel, 1950; Lowe, 1969; Takahashi et al., 1974; Lowe and Turnbull, 1995*]. Among the variety of available airglow emissions, the OH Meinel bands are the most frequently used feature because of the well-dispersed rotational lines of the vibrational bands, and its extension and intensity in the airglow spectrum (from 400 nm to 4 μm and with the total nightglow intensity estimated to be about 1.3 MR). These characteristics make possible the accurate determination of the vibrationally excited OH (hereinafter referred to as

OH\*) rotational temperatures with spectrometers of moderate resolution. One concern with hydroxyl rotational temperature measurement is the validity of the assumption of thermal equilibrium for the rotational levels. *Pendleton et al.* [1993] have shown that for high rotational quantum numbers the OH\* rotational populations can strongly deviate from the thermal equilibrium values. However, the same work has also indicated the validity of the assumption of thermal equilibrium for lower rotational levels ( $N < 4$ ). Most recent ground-based temperature measurements using the OH Meinel bands have been used primarily to investigate dynamical processes (*Meriwether* [1989] summarizes pre-1989 work; *Hecht et al.* [2000] is a more recent example). In fact, the data that have been accumulated over nearly a half a century constitute a unique source for the study of long-term changes in the upper mesosphere region.

Ground-based airglow observations, however, usually do not contain altitude information. With the development of the sodium temperature lidar, it has become possible to determine the temperature profile from about 80 to 105 km altitude by detecting the thermally Doppler broadened NaD<sub>2</sub> resonance structure [*Fricke and von Zahn, 1985*]. Subsequently, lidar

---

<sup>1</sup> Now at Department of Physics, University of Toronto, Toronto, Ontario, Canada.

temperature observations have made major contributions to our understanding of the temperature structure of the mesopause region. Examples are the observation of the bimodal character of the mesopause altitude [von Zahn *et al.*, 1996 ; She and von Zahn, 1998 ] and the occurrence of temperature inversion layers also above 85 km [Dao *et al.*, 1995; States and Gardner, 1998]. The lidar data, however, do not normally provide direct information about any horizontal structures present in the upper mesosphere region. Such information can be obtained from airglow imager observations [e.g., Taylor, 1997].

The first attempt to make simultaneous measurements using the two techniques was made by von Zahn *et al.* [1987]. They used colocated lidar and airglow measurements to determine the altitude of the hydroxyl layer through comparison of the two independent temperature measurements. The technique was applied to three nights of measurement taken in January of 1986 at the Andoya Rocket Range (69°N, 16°E). The OH (3-1) band airglow layer was found to be at an altitude of  $86 \pm 4$  km, a result in good agreement with the rocket and satellite observations. However, in comparisons of the 86-km lidar equivalent layer temperature with the OH\* rotational temperature, von Zahn and coworkers found differences of up to 10 K when hourly averaged data were used. These differences were discussed in terms of possible interference from passing clouds, the larger field of view of the OH spectrometer compared with the lidar beam, the possible existence of rapid vertical motions of the OH\* layer driven by gravity waves, and the assumed OH\* layer shape.

More recently this combination of methods was applied by She and Lowe [1998] to a larger data set extending over 1 year. On the basis of 51 nights of sodium lidar data over Fort Collins (41°N) and 78 nights of Fourier transform spectrometer data taken over the Delaware Observatory (43°N) during 1993, the OH (3-1) rotational temperatures and the Na lidar temperature in the mesopause region were analyzed and compared statistically. She and Lowe found that OH rotational temperatures inferred from the convolution of the lidar observed temperature profiles with WINDII/UARS OH\* (8-3) P1(3) height profiles over Fort Collins (41°N, 105°W) were in general agreement with the lidar temperatures at  $87 \pm 3$  km. The monthly mean rotational temperatures inferred in this way from the lidar observations were in statistical agreement with the hydroxyl rotational temperatures observed over the Delaware Observatory at the same latitude but 24° to the east. A direct comparison of the airglow temperatures showed that they were a useful proxy for the 87-km temperature as observed by the lidar.

In fact, one should keep in mind that the association of the measurement of the OH\* rotational temperature with neutral temperature depends on the shape of the OH\* height profile. The OH\* airglow has been normally assumed to be a single layer with a peak between 85 and 90 km. Such an assumption has been confirmed from the hydroxyl measurements made by the WINDII experiment on board the UARS satellite. However, in a detailed study of the OH\* profiles obtained by the WINDII instrument

since the end of 1991, Melo *et al.* [2000] observed that from 5 to 25% of the measured profiles have a more complex structure for the layer profile, most frequently with two peaks separated by 4-6 km. Such structures have a horizontal extension from 200 to several thousand kilometers and can persist for as long as 12 hours. The frequency of occurrence of such structures was found to be dependent on season, latitude, and local time. Melo and coworkers suggest that although gravity waves could be the source of isolated small-scale events of this type, the long-duration structures are more likely to result from temperature inversion layers or mixing events (or a combination of both).

A mesosphere inversion layer (MIL) is an inversion in the gradient of the mesospheric temperature profile often characterized by a large temperature enhancement (typically 10-25 K but can be as high as 100 K) above nominal temperature profile values [Dao *et al.*, 1995; Meriwether *et al.*, 1994]. These temperature anomalies are generally located between 70 and 90 km with a width of about 10 km. The MILs have been observed to last for several hours at a given location and even appear in monthly averaged profiles. The origin of the MILs is not clear yet. Dynamical heating due to gravity wave breaking, chemical heating events, large-amplitude waves, and transition from summer to winter mesopause are among the proposed mechanisms. In addition, the role that tides and planetary waves could play in the formation of the MIL is not yet understood. It is believed that gravity wave activity plays an important role in developing a link between the MILs and tides through coupling of gravity wave and the tide resulting in an amplification of the tidal thermal structure [e.g., Meriwether and Gardner, 2000; Meriwether *et al.*, 1998; States and Gardner, 1998]. Indeed, a downward propagation with phase speed representative of tides has been observed. However, the enhancement in temperature observed in a temperature inversion event is considerably larger than predicted [Hagan *et al.*, 1997; Meriwether and Gardner, 2000] using the global-scale wave model, which includes the effect of gravity wave interactions with tidal structures.

As shown by Swenson and Gardner [1998] and Gardner and Taylor [1998], the cancellation of the induced perturbation in the hydroxyl intensity and rotational temperature is significant for gravity waves with short vertical wavelength ( $\lambda_z \leq 12$  km). Therefore such waves may not be detectable from observations of the hydroxyl integrated intensities. We note that this would not be the case for the most commonly observed tidal modes (diurnal, semidiurnal, 8 hour, etc.) since they have typical vertical wavelengths larger than 12 km. Indeed, the impact of a strong localized temperature enhancement, such as observed in an inversion layer, on the observations of the OH\* rotational temperature taken in a zenith configuration has not been addressed previously.

We show here that because of the temperature dependence of the reaction rates in the HO<sub>x</sub> chemistry, nights with unusual temperature profiles such as caused by an extreme temperature inversion layer can lead to severe alteration of the OH\* height profile. On such

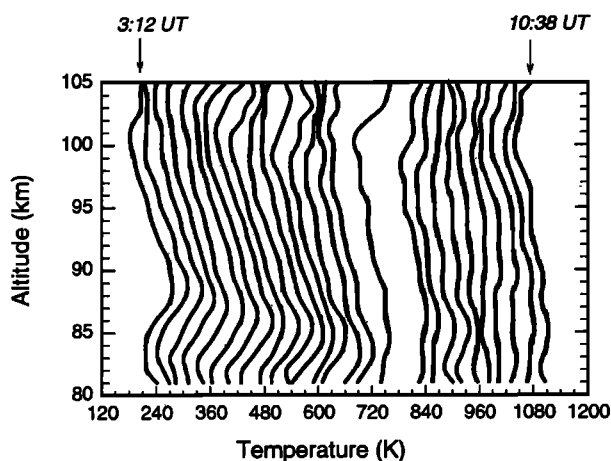


**Figure 1.** Lidar measurements of the temperature profile as a function of altitude for each 15 min from 0312 UT to 1038 UT. Except for the first profile, the temperatures are up-shifted by 30 K sequentially for each profile for clarity.

occasions, OH\* temperatures measured by a ground-based instrument may no longer be a reliable proxy for the temperatures at 87 km. To illustrate the mechanisms involved and the sensitivity to the chemical reaction rates, we investigate a dramatic mesospheric temperature enhancement event observed by the Na lidar at Fort Collins (41°N, 105°W) on the night of November 2-3, 1997 (day 307).

During this night the mean (average of hourly means) temperature at 87 km reached 249 K, compared with the November-February mean for 1993 of 220 K [She and Lowe, 1998] and the 7-year climatological mean at 87 km of 216 K. Making this study possible is the fact that the Utah State University OH\* mesospheric temperature mapper (MTM) was colocated with the Na lidar at Fort Collins from July 1997 to June 1998 [Taylor et al., 1999]. The seasonal variation of the nightly mean of the MTM temperatures and the lidar temperature at 87 km were compared and found to be in good agreement (see section 2.3 for more details) except for this one night in which the MTM nightly mean temperature was determined to be 32 K lower than the lidar temperature at 87 km. The largest difference was observed at 0438 UT when the MTM and lidar temperatures were 235 and 281 K, respectively. To place these measurements in perspective, we point out that this night exhibited the highest nightly mean temperature over the 9-year span (1990 to March 1999) of lidar temperature measurements from Fort Collins. Among the 417 nights of data, there are only four other nights with nightly means higher than 240 K and 30 nights higher than 225 K.

The temperature profiles measured by the Na lidar in 15-min intervals within 1-km resolution are used here to evaluate the resulting perturbations in OH\* height profiles based on a current photochemical model. Using the OH\* height profiles so calculated, we deduce the corresponding time series of OH (6-2) integrated intensities and hence infer rotational temperatures. These OH\* integrated intensities and rotational temperatures are then compared with those measured by the MTM.

## 2. Observations

### 2.1. Lidar Observed Temperature Enhancement

Figure 1 shows the time series of the lidar temperature profiles observed on the night of November 2-3 of 1997. They are 15 min apart and are up-shifted by 30 K sequentially for each profile. A well-defined temperature inversion layer centered at 89 km at 0312 UT can be identified from the figure. The layer moves downward with time, moving out of the altitude range of the lidar at about 0688 UT. The maximum and minimum temperatures at 87 km occur at 0438 and 0962 UT, respectively. The lidar temperature profiles at these times are shown in Figure 2 along with the 7-year climatological and the mass spectrometer/incoherent scatter (MSIS) nightly mean temperature profiles for comparison. The differences between the MSIS and 7-year lidar climatology and the measured temperature at 87 km at 0438 UT are 88 and 65 K, respectively. Notice that the measured temperature at 0962 UT and the 7-year mean are in agreement, giving an observed maximum enhancement of 65 K. This unusual and dramatic temperature enhancement observed this night is intriguing. Although the occurrence of MIL has been observed at different locations, the mechanism responsible for its generation is still not understood [Whiteway and Carswell, 1995; Meriwether and Mlynczak, 1995; States and Gardner, 1998; Huang et al., 1998]. An analysis of the data set presented here in terms of the causes for the temperature enhancement and the implication of the observed large-amplitude temperature perturbation with regions of convective instability is now in progress.

### 2.2. MTM Measured OH(6-2) Rotational Temperatures and Intensities

The MTM data for both the OH (6-2) rotational temperature and integrated intensity are shown in Figure

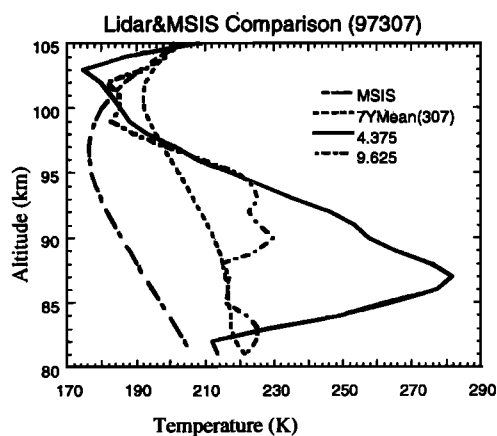


**Figure 2.** The temperature profiles at the peak (end) of the temperature enhancement at 0438 UT (0962 UT) compared with mass spectrometer/incoherent scatter (MSIS) model results nightly and 7-year lidar nighttime mean for day 307.

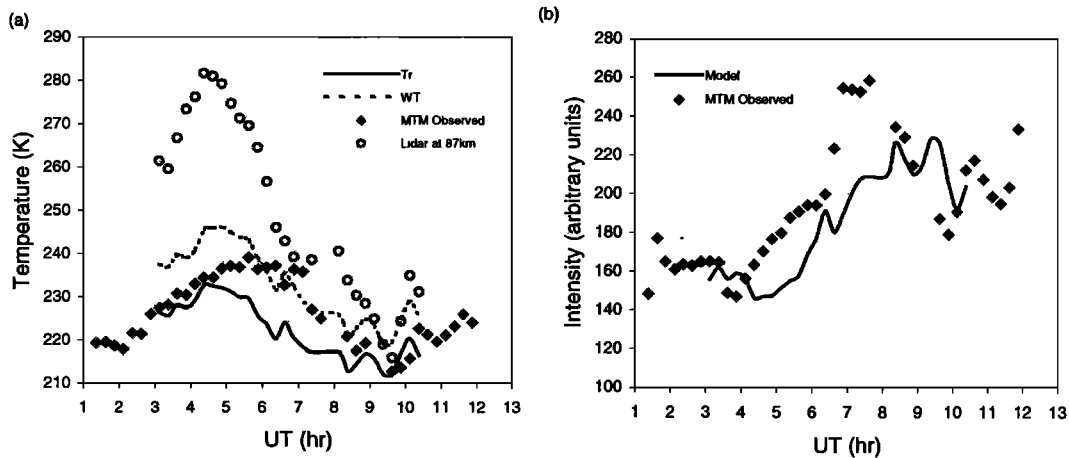


**Figure 3.** Time evolution of the (a) temperature measured by the mesospheric temperature mapper (MTM) imager (diamonds), measured by the Na lidar at 87 km (open circles), and calculated OH (6-2) R (solid line) and OH (6-2) W (broken line) and (b) OH (6-2)  $P_1(2)$  line integrated intensity measured by the MTM imager (diamonds) and calculated from the model (solid line).

3a and 3b. (A description of the MTM data used here including time resolution, accuracy/precision, field of view, etc., is given by *Taylor et al.* [1999]. The OH\* integrated intensities are given in arbitrary units since the MTM instrument was not absolutely calibrated. For comparison, we include in Figure 3a the variation in temperature measured by the lidar at 87 km.

### 2.3. Comparison of Temperature Results From the Two Techniques

When the MTM started observing at 0144 UT, it measured a rotational temperature of 217 K: The lidar observations start at 0312 UT when it indicated a temperature of 261 K. At 0312, when both instruments were operating, the MTM measurements indicate a temperature lower by 42 K. At 0438 UT the lidar temperature reached maximum and the MTM measured a temperature 46 K colder. Although the MTM observations initially showed an increase in temperature with a maximum of 228 K at 0600 UT, the temperature measured by MTM was always lower than the lidar temperatures at 87 km, except at ~0930 UT, when they are about the same.

The nocturnally averaged OH M (6-2) rotational temperature observed from the MTM was 226 K (with a standard deviation of about 8 K) while the lidar-averaged temperature at 87 km was about 250 K. In comparison, an unoptimized study of the MTM and lidar temperatures for 12 nights of overlapping data (average length ~ 7.5 hours) during the 6-month period June-December 1997 (seasonal temperature range ~175-215 K) yielded a correlation coefficient  $r$  of 0.96 and a mean nightly difference of only 0.6 K. However, variations on a night-by-night basis indicate that the MTM nightly means (referenced to the lidar-derived 87-km temperatures) were compatible to about  $\pm 5$  K [*Taylor et al.*, 2001]. Therefore the nocturnal averaged 87-km lidar temperature data significantly exceeded the OH\* temperature (by ~ 24K),

suggesting that a major departure from the normal airglow emission occurred on this occasion.

A precise comparison between the lidar temperature and the hydroxyl rotational temperature requires knowledge of the height profile of the airglow emission [*von Zahn et al.*, 1987; *She and Lowe* 1998] used monthly mean profiles of the volume emission rate from WINDII/UARS for this purpose. The use of averaged emission rate profiles is not appropriate here because the large deviation of the temperature profile can strongly impact the shape of the hydroxyl profile, leading to significant deviations from its average shape.

Looking only at the MTM data, one can clearly identify an ~8-hour oscillation in both the temperature and the intensity [*Taylor et al.*, 2001]. Assuming a model to describe the OH airglow response to a gravity wave based on the model proposed by *Swenson and Gardner* [1998] with the photochemistry as described below, we found that the observed phase difference of approximately  $-90^\circ$  between the temperature and the intensity oscillations is roughly reproduced assuming a monochromatic wave with vertical wavelength of about 25 km. Note that the structure observed in the lidar temperature has a width of about 10 km.

Using a larger data set, *Taylor et al.* [1999] have observed that the presence of ~8-hour oscillations is a common feature in the OH\* rotational temperature observations at both Bear Lake Observatory, Utah (41.9°N, 111.6°W), and Fort Collins, Colorado (40.6°N, 105°W), during the equinox months. The authors found that the respective amplitude and phase for the observed 8-hour oscillation are in good agreement with the lidar climatology for an altitude of 87 km. However, *Taylor et al.* [1999] also found that for the night of November 2-3, 1997 (the one under investigation here), the amplitude of the 8-hour oscillation at the OH\* rotational temperature exceeded the lidar climatology by a factor of 2.

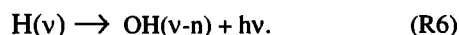
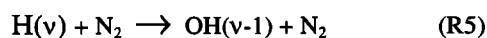
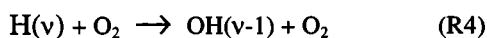
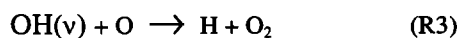
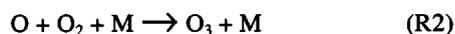
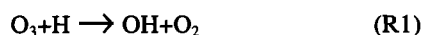
**Table 1.** Rate Constants Used in the OH( $\nu$ ) Chemical Model<sup>a</sup>.

Reaction	Coefficient	Comments
(R1)	$1.4 \times 10^{-10} \exp(-470/T) f(\nu)$	$f(9)=0.48; f(8)=0.27;$ $f(7)=0.17;$ $f(6)=0.08$
(R2)	$6.0 \times 10^{-34} (300/T)^{2.3}$	
(R3)	$2.5 \times 10^{-10}$	see comments in text
(R4)	$c_9(\nu) \times 10^{-13}$	$c_9(9)=170; c_9(8)=98;$ $c_9(7)=54;$ $c_9(6)=30$
(R5)	$c_{10}(\nu) \times 10^{-14}$	$c_{10}(9)=48; c_{10}(8)=27;$ $c_{10}(7)=16;$ $c_{10}(6)=9.1$

<sup>a</sup>The coefficients' values are the same as those of *Makhlouf et al.* [1995], and the units are  $\text{cm}^3 \text{s}^{-1}$  for a two-body reaction and  $\text{cm}^6 \text{s}^{-1}$  for a three-body reaction.

### 3. Photochemical Model

Our approach is to use a one-dimensional (1-D) photochemical model extracted from *Makhlouf et al.* [1995] comprising the following set of reactions:



The OH is formed through the exothermic reaction between ozone and hydrogen (R1) that can excite vibrational levels of hydroxyl up to the  $\nu=9$  level. Through the upper mesosphere the ozone formation is the result of the three-body recombination of atomic oxygen (R2). The main nonradiative OH\* loss occurs via (R3)-(R5), quenching with  $\text{O}_2$  and  $\text{N}_2$  and chemical reaction with O, the latter process being important only for the lower vibrational levels. Reaction (R1) is the main destruction process of ozone at night in the mesopause region. Hence the OH\* emission rate depends only on atomic oxygen concentration and the background atmosphere ( $\text{O}_2$  and  $\text{N}_2$  concentrations and neutral temperature  $T$ ). The dependence on temperature results mainly from the temperature variation of the rate coefficients for ozone destruction and production (reactions (R1) and (R2) (see Table 1). Because of the short lifetime of the OH\* molecule ( $\ll 1$  s), disturbances in the volume emission rate occur indirectly through disturbances in O,  $\text{O}_2$ ,  $\text{N}_2$ , and T.

The rate constants for (R1)-(R5) are listed in Table 1. The branching ratios for populating each vibrational level through (R1) were taken from *Klenerman and Smith* [1987]. One of the difficulties in describing the OH\* chemistry is the fact that many of the required quenching rate constants are uncertain. Although laboratory works indicated that  $\text{O}_2$  is more efficient than  $\text{N}_2$  in deactivating OH\*, the set of measured values is still incomplete.

Consequently, some assumptions must be made. Following *Makhlouf et al.* [1995], the rate constants for quenching by  $\text{O}_2$  (R4) are taken from *Dodd et al.*, [1991] for  $\nu = 6$ , from *Knutsen and Copeland* [1993] for  $\nu = 7$  and  $\nu = 8$ , and from *Chalamala and Copeland* [1993] for  $\nu = 9$ . For quenching by  $\text{N}_2$  (R5), we use the rate constants determined by *Makhlouf et al.* [1995] through interpolation between measurements at  $\nu=2$  and  $\nu=12$ . Note that quenching has a greater effect on the lower vibrational levels, since they have a longer lifetime.

The reaction between OH and O (reaction (R3)) constitutes another difficulty in modeling the hydroxyl airglow. There are no experimental values for OH ( $\nu = 2$ ) up to OH ( $\nu = 9$ ). However, airglow observations have suggested the importance of this process, and an empirical value as high as  $4.0 \times 10^{-10} \text{ cm}^3 \text{ s}^{-1}$  has been suggested [*Sivjee and Hamwey*, 1987]. Again, following *Makhlouf et al.* [1995], we have adopted the gas kinetic collisional upper limit ( $2.5 \times 10^{-10} \text{ cm}^3 \text{ s}^{-1}$ ).

To determine an equilibrium height profile using (R1)-(R5), in addition to the temperature profiles provided by lidar observation, we need  $\text{N}_2$ ,  $\text{O}_2$ , and O concentration profiles; these are taken from the MSIS model of *Hedin et al.* [1991] for the same local time where the temperature profiles are available from the lidar observations. Observe that the MSIS model output for the altitude range of interest here shows only minor contribution of atmospheric tides. At the mesopause region the long chemical lifetime of the atomic oxygen ensures that the changes in the number density are determined by vertical transport rather than by the effect of temperature changes in the reaction rates. If the observed perturbation were purely gravity wave or tidally driven, then we would expect the temperature and [O] perturbation to be essentially in phase in the primary OH M region. Indeed, most of the proposed mechanisms for generating the MILs involve changes in the dynamical field [e.g., *Liu et al.*, 2000]. However, in the current case it is unclear what changes would be expected in the atomic oxygen density profile since the dominant forcing mechanism has not been completely identified. This said, we anticipate no significant impact on our results by increasing or decreasing the total amount of atomic oxygen along the altitude profile without changing the gradient of the bottomside of the layer. Nor will a small shift in altitude (e.g., by  $\sim 1$  km) of the atomic oxygen peak density significantly affect the results presented here.

The photochemical model generates OH\* volume emission profiles for the same latitude and longitude, day of year, and time of day as for the temperature profiles observed from the lidar. Therefore the model is run for each available temperature profile producing the respective OH\* volume emission rate profile. Figure 4 shows the calculated OH (6-2) volume emission rate (VER) as a function of altitude and time (UT). Note that the profiles are 15 min apart and are shifted by 450 photons  $\text{cm}^{-3} \text{ s}^{-1}$  sequentially for clarity. Examining this figure against the unusual structures in temperature in Figure 1, we note that strong changes in the shape and peak altitude of the hydroxyl height profile have resulted in response to extreme temperature enhancement and that

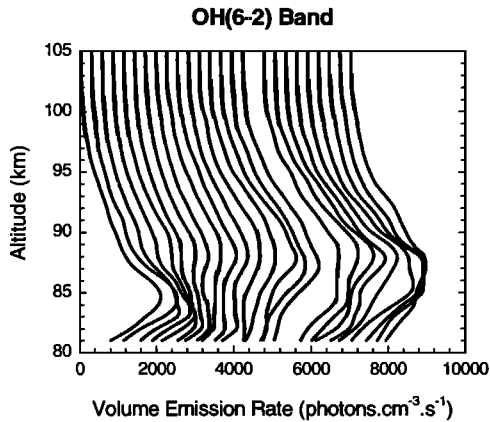


**Figure 4.** Time evolution of the OH(6-2) volume emission rate as a function of altitude, calculated using the measured temperature profiles. The profiles are shifted by  $450 \text{ photons cm}^{-3} \text{ s}^{-1}$  and are 15 min apart. The horizontal scale refers only to the first curve (0312 UT).

the hydroxyl volume emission rate decreases when the temperature increases. Such an effect comes from the dependence of the hydroxyl nightglow excitation on the oxygen recombination reaction (R2) which is temperature dependent:  $k = 6.0 \times 10^{-34} (300/T)^{23} \text{ cm}^6 \text{ s}^{-1}$ .

#### 4. Calculated and MTM Measured OH\* Airglow Intensity and Rotational Temperature

We calculate the rotational temperature for the OH (6-2) bands through the ratio between the integrated intensity of the  $P_1(2)$  and  $P_1(4)$  rotational lines. The ratios of the integrated intensities of these lines are calculated, from which the rotational temperature ( $T_{\text{rot}}$ ) is then deduced using

$$T_{\text{rot}} = \frac{E_b - E_a}{k \ln(I_a A_b g_b / I_b A_a g_a)}, \quad (1)$$

where  $k$  represent the Boltzmann's constant,  $a$  and  $b$  represent the two rotational states,  $E_{a,b}$  represent the energy of specified vibrational-rotational level,  $I_{a,b}$  represent the integrated intensity of the rotational line,  $A_{a,b}$  represent the transition probabilities taken from *Turnbull and Lowe*, [1989], and  $g_{a,b}$  represent the degeneracy factor for the specific rotational line. We refer the rotational temperature ( $T_{\text{rot}}$ ) so deduced as OH (6-2) R. This is expected to be what a ground-based instrument measures. Alternatively, we may calculate the OH\* rotational temperature ( $T_{\text{rot}}$ ) from the lidar-measured temperature profiles weighted by the calculated OH height profile; we refer to such rotational temperatures as OH (6-2) W.

The simulated OH (6-2) rotational temperatures, both OH (6-2) R and OH (6-2) W, are shown in Figure 3 as a function of time (UT), together with the MTM observations of the OH (6-2) rotational temperature and the lidar temperature at 87 km. As can be seen from the figure, the calculated OH (6-2) R and OH (6-2) W are in

general agreement, with the calculated OH (6-2) W being higher than calculated OH (6-2) R by 1-5 K. Compared with the MTM temperatures, both calculated OH (6-2) R and OH (6-2) W are in good agreement with OH (6-2) R in better agreement before 0500 UT and OH (6-2) W better between 0500 and 0800 UT. As mentioned before, the centroid height of the hydroxyl nightglow layer is normally located at about 87 km. However, as can be seen from Figure 4, that is clearly not the case for the night of November 2-3, 1997. The model results show that in fact the presence of such strong structure in the temperature profile alters the shape of the OH\* layer, moving the altitude of the centroid of the OH\* layer. With time, as the structure moves in altitude, the centroid of the OH\* layer also moves in altitude, making the OH\* rotational temperature differ from the lidar temperature observed at about 87 km.

In this work we have considered only the effects of the temperature changes on the airglow emission. Other factors related to changes in the density of either the major or the minor (or major and minor) constituents are potentially significant, but, as the mechanism responsible for the MIL has not been clearly identified, any assumptions on their variation during this unusual event would be arbitrary at this stage. However, it is interesting to examine how the model used here works for the OH\* integrated intensity. The temporal evolution of the modeled integrated intensity for the OH (6-2)  $P_1(2)$  line is shown in Figure 3 together with the MTM observations for the same line. Note that since the MTM intensity data were not calibrated absolutely, the model results were scaled (by a constant factor) to the MTM values. As can be seen from Figure 3, the nocturnal variation of the modeled intensities compares reasonably well with the observed OH\* intensity. Such agreement reinforces the results for the OH\* rotational temperature obtained with the photochemical model assumed here.

Since it is clear that the mesospheric temperature inversion layer and tides are linked somehow, and as tides are a strong dynamical feature of the mesospheric region, the potential for many examples such as the one described here exists. However, previous work [e.g., *She and Lowe*, 1998; *Taylor et al.*, 2001] has shown evidence that the OH airglow measurements can, in most of the cases, be used as a good proxy for the ~87-km temperature in the upper mesosphere. The results presented here clearly refer to an extreme case, which is far from the usual situation. However, they emphasize the need for a better understanding of the processes involved in the generation of MILs in order to properly understand and interpret their impact on the airglow emissions. Although such extreme temperature enhancement events may be rare at midlatitudes, they may impact the analysis of airglow observations in terms of both global and long-term effects.

#### 5. Conclusion

Ground-based measurements of the integrated intensity of the different rotational lines of the hydroxyl nightglow have been used extensively to infer the atmospheric temperatures at the upper mesosphere altitudes, shown

previously to be at ~87 km. However, during extreme perturbations, the height profile of the OH\* volume emission rate may be altered significantly, compromising the correct interpretation of these measurements due to the lack of information about the altitude distribution of the nightglow volume emission rate.

In the present work we have investigated an unusual temperature enhancement event on the night of November. 2-3, 1997, over the mesopause region observed from Fort Collins, Colorado (41°N, 105°W). During this night, an OH mesospheric temperature mapper (MTM) was colocated and operated beside the Na temperature lidar. Throughout the night, the measured OH temperatures were lower, by as much as ~45 K at 0438 UT. To explain this very large discrepancy, we have used a current one-dimensional photochemical model, the lidar measured temperature profiles, and MSIS N<sub>2</sub>, O<sub>2</sub>, and O densities to simulate the OH\* height profiles and OH (6-2) rotational temperature. The high-temperature perturbation was shown to impact the photochemistry of OH and O<sub>3</sub> and to severely alter the OH\* height profiles. The simulated temperatures exhibit a time series in general agreement with the temperatures measured by the colocated MTM. The magnitude of the predicted intensity and temperature perturbations were in clear agreement with the measured values. However, the observed phase (~90°) and modeled phase (~180°) relationships were in relatively poor agreement and probably reflect the (currently unknown) contribution of the [O] dynamics to the total OH M intensity perturbation.

In summary, this study suggests that under unusually strong temperature perturbations, photochemical processes of OH and O<sub>3</sub> play an important role in the background state parameters and in determining the OH\* height profiles in the mesopause region. As a result we advise caution in using airglow signatures for the measurement of background atmospheric parameters under a strongly perturbed atmospheric condition.

**Acknowledgments.** The authors thank Dave Krueger for useful discussions. This work was partially supported by the Centre for Research in Earth and Space Technology, Ontario. The Colorado State University Na lidar measurements were supported by the National Science Foundation under grants ATM 96-12832 and ATM 97-14676, and the Utah State University CEDAR MTM measurements were supported under grant ATM 96-12810.

Janet G. Luhmann thanks John W. Meriwether and another referee for their assistance in evaluating this paper.

## References

- Chalamala, B.R., and R.A. Copeland, Collision dynamics of OH(X<sup>2</sup>Π, v=9), *J. Chem. Phys.*, 99(8), 5807-5811, 1993.
- Dao, P.D., R. Farley, X. Tao, and C.S. Gardner, Lidar observations of the hyperfine structure of the D2 resonance line of sodium by lidar, *J. Atmos. Terr. Phys.*, 47, 499-512, 1985.
- Fricke, K.H., and U. von Zahn, Mesopause temperatures derived from probing the hyperfine structure of the D2 resonance line of sodium by lidar, *J. Atmos. Terr. Phys.*, 47, 499-512, 1985.
- Gardner, C.S., and M.J. Taylor, Observational limits of lidar, radar, and airglow imager measurements of gravity wave parameters, *J. Geophys. Res.*, 103, 6427-6437, 1998.
- Hagan, M.E., C. Mclandress, and J.M. Forbes, Diurnal tidal variability in the upper mesosphere and lower thermosphere, *Ann. Geophys.*, 15, 1176-1186, 1997.
- Hecht, J.H., C. Fricke-Begemann, R.L. Walterscheid, and J. Hoffner, Observations of the breakdown of an atmospheric gravity wave near the cold summer mesopause at 54°N, *Geophys. Res. Lett.*, 27, 879-882, 2000.
- Hedin, A.E., et al., Revised global model of thermospheric winds using satellite and ground-based observations, *J. Geophys. Res.*, 96, 7657-7688, 1991.
- Huang, C.S., G.J. Sofko, and M.C. Kelley, Numerical simulations of midlatitude ionospheric perturbations produced by gravity waves, *J. Geophys. Res.*, 103, 6977-6989, 1998.
- Klenerman, D., and I.W.M. Smith, Infrared chemiluminescence studies using a SISAM spectrometer, *J. Chem. Soc. Faraday Trans.*, 2, 83, 229, 1987.
- Knutsen, K., and R.A. Copeland, Vibrational relaxation of OH(X<sup>2</sup>Π, v=7,8) by O<sub>2</sub>, N<sub>2</sub>, N<sub>2</sub>O and CO<sub>2</sub>, *Eos Trans. AGU*, 74, Fall Meet. Suppl., 472, 1993.
- Liu, H.-L., M. E. Hagan, and R.G. Roble, Local mean state changes due to gravity wave breaking modulated by the diurnal tide, *J. Geophys. Res.*, 105, 12,381-12,396, 2000.
- Lowe, R.P., Interferometric spectra of the Earth's airglow (1.2 to 1.6 um), *Philos. Trans. R. Soc., London, Ser. A*, 264, 164-169, 1969.
- Lowe, R.P., and D.N. Turnbull, Comparison of ALOHA-93, ANLC-93, and ALOHA-90 observations of the hydroxyl rotational temperature and gravity wave activity, *Geophys. Res. Lett.*, 22, 2813-2816, 1995.
- Makhlouf, U.B., R.H. Picard, and J.R. Winick, Photochemical-dynamical modeling of the measured response of airglow to gravity waves, 1, Basic model for OH airglow, *J. Geophys. Res.*, 100, 11,289-11,312, 1995.
- Meinel, A.B., OH emission bands in the spectrum of the night sky, I, *Astrophys. J.*, 111, 555, 1950.
- Melo, S.M.L., R.P. Lowe, and J.P. Russel, Double-peaked hydroxyl airglow profiles observed from WINDII/UARS, *J. Geophys. Res.*, 105, 12,397-12,403, 2000.
- Meriwether, J.W., A review of the photochemistry of selected nightglow emission from the mesopause, *J. Geophys. Res.*, 94, 14,629-14,646, 1989.
- Meriwether, J.W., and C.S. Gardner, A review of the mesosphere inversion layer phenomenon, *J. Geophys. Res.*, 105, 12,405-12,416, 2000.
- Meriwether, J.W., and M.G. Mlynczak, Is chemical heating a major cause of the mesospheric inversion layer?, *J. Geophys. Res.*, 100, 1379-1387, 1995.
- Meriwether, J.W., P.D. Dao, R.T. McNutt, W. Klemetti, W. Moskowitz, and G. Davidson, Rayleigh lidar observations of mesosphere temperature structure, *J. Geophys. Res.*, 99, 16,973-16,987, 1994.
- Meriwether, J.W., X. Gao, V.B. Wickwar, T. Wilkerson, K. Beissner, S. Collins, and M.E. Hagan, Observed coupling of the mesospheric inversion layer to the thermal tidal structure, *Geophys. Res. Lett.*, 25, 1479-1482, 1998.
- Pendleton, W.R., P.J. Espy, and M.R. Hammond, Evidence for non-local-thermodynamic-equilibrium rotation in the OH Nightglow, *J. Geophys. Res.*, 98, 11567-11579, 1993.
- She, C.-Y., and U. von Zahn, Concept of a two-level mesopause: Support through new lidar observations, *J. Geophys. Res.*, 103, 5855-5863, 1998.
- She, C.-Y., and R.P. Lowe, Seasonal temperature variations in the mesopause region at mid-latitude: Comparison of lidar and hydroxyl rotational temperatures using WINDII/UARS height profiles, *J. Atmos. Sol. Terr. Phys.*, 60, 1573-1583, 1998.
- Sivjee, G.G., and R.M. Hamwey, Temperature and chemistry of the polar mesopause OH, *J. Geophys. Res.*, 92, 4663-4672, 1987.
- States, R.J., and C.S. Gardner, Influence of the diurnal tide and thermospheric heat sources on the formation of mesospheric temperature inversion layers, *Geophys. Res. Lett.*, 25, 1483-1486, 1998.
- Swenson, G.R., and C.S. Gardner, Analytical models for the responses of the mesospheric OH\* and Na layers to atmospheric gravity waves, *J. Geophys. Res.*, 103 (D6), 6271-6294, 1998.
- Takahashi, H., B.R. Clemesha, and Y. Sahai, Nightglow OH (8,3) band intensities and rotational temperature at 23 S, *Planet. Space Sci.*, 22, 1323-1329, 1974.

- Taylor, M.J., A review of advances in imaging techniques for measuring short-period gravity waves in the mesosphere and lower thermosphere, *Adv. Space Res.*, 19, 667-676, 1997.
- Taylor, M.J., W.R. Pendleton Jr., C.S. Gardner, and R.J. States, Comparison of terdiurnal tidal oscillations in mesospheric OH rotational temperature and Na lidar temperature measurements at mid-latitudes for fall/spring conditions, *Earth Planets Space*, 51, 877-885, 1999.
- Taylor, M.J., L.C. Gardner, and W.R. Pendleton Jr., Long-period wave signatures in mesospheric OH Meinel (6,2) band intensity and rotational temperature at mid-latitudes, *Adv. Space Res.*, in press, 2001.
- von Zahn, U., K.H. Fricke, R. Gerndt, and T. Blix, Mesospheric temperatures and the OH layer height as derived from ground-based lidar and OH\* spectrometry, *J. Atmos. Terr. Phys.*, 49, 863-869, 1987.
- von Zahn, U., J. Hoffner, V. Eska, and M. Alpers, The mesopause altitudes: Only two distinctive levels worldwide?, *Geophys. Res. Lett.*, 23, 3231-3234, 1996.
- Whiteway, F.A., and A.I. Carswell, Lidar observations of gravity wave activity in the upper stratosphere over Toronto, *J. Geophys. Res.*, 100, 14,113-14,124, 1995.

---

R. P. Lowe, University of Western Ontario, London, Canada N6A 3K1.

Stella M. L. Melo, Department of Physics, University of Toronto, Toronto, Ontario, Canada M5S 1A7. (stella@atmosph.physics.utoronto.ca)

W. R. Pendleton Jr. and M. J. Taylor, Space Dynamics Laboratory, Utah State University, Logan, UT 84341, UAS.

C. Y. She and B. Williams, Colorado State University, Fort Collins, CO 80523, USA.

(Received January 16, 2000; revised August 22, 2001; accepted August 23, 2001.)